OPEN ACCESS Freely available online

ISSN 2737-5323
Volume 5, Issue 4
https://afm.iikii.com.sg
Applied Functional Materials

Article

Rapid Flash Paper Combustion Synthesis of Cobalt Blue Pigment Nanoparticles for Use in Color 3D Printing Formulations

Athanasios B. Bourlinos [1,*], Alexandros Polymeros [1], Christina Papachristodoulou [1], Dimitrios Moschovas [2], Apostolos Avgeropoulos [2], Constantinos E. Salmas [2], and Michael A. Karakassides [2]

[1] Physics Department, University of Ioannina, Ioannina 45110, Greece; apolimer@uoi.gr (A. P.), xpapaxri@uoi.gr (C. P.)
[2] Department of Materials Science & Engineering, University of Ioannina, Ioannina 45110, Greece; dmoschov@uoi.gr (D. M.), aavger@uoi.gr (A. A.), ksalmas@uoi.gr (C. E. S.), mkarakas@uoi.gr (M. A. K.)
* bourlino@uoi.gr; Tel.: +30 2651 008511

Received: Jul 17, 2025; **Revised:** Jul 28, 2025; **Accepted:** Aug 02, 2025; **Published:** Dec 30, 2025

Abstract: This study introduces a broadly applicable and potentially scalable method for synthesizing pigment nanoparticles, using a novel solution combustion approach termed flash paper combustion. The method is demonstrated through the preparation of cobalt blue nanopigment (cobalt aluminate, $CoAl_2O_4$) by impregnation of nitrocellulose-based flash paper substrates in a stoichiometric solution of metal nitrates, followed by mild drying. Upon ignition, the flash paper facilitated a rapid, self-sustained combustion reaction, resulting within a few seconds in a lightweight, cobalt blue nanopowder with consistent yield and appearance across samples. The synthesized material was characterized by X-ray diffraction (XRD), transmission electron microscopy (TEM), and nitrogen porosimetry. Structural and morphological analyses verified the formation of a crystalline cubic spinel phase, consisting mainly of nearly spherical nanoparticles with an average size of 20 nm and a specific surface area of 51 $m^2 g^{-1}$. The method offers an efficient approach for synthesizing nanoscale $CoAl_2O_4$, showing promise for pigment applications in 3D printing formulations, where the nanoparticles can be easily dispersed without pre-treatment in suitable photoactive resin matrices, enabling the creation of vividly colored artifacts of any type.

Keywords: Solution combustion synthesis, Flash paper, Nitrocellulose, Metal nitrates, Cobalt blue, Nanoscale pigments, Color 3D printing

1. Introduction

Solution combustion synthesis (SCS) is a versatile and efficient bottom-up method for producing nanoparticles, especially binary and ternary metal oxides-such as simple oxides, spinels, and perovskites-that exhibit valuable optical, magnetic, electronic, and biomedical properties [1–5]. In this method, a metal precursor, typically a nitrate, is combined with an organic fuel like glycine, urea, or citric acid in an aqueous solution. After drying into a xerogel, the mixture is ignited, triggering a highly exothermic reaction that rapidly generates fine, crystalline nanoparticles. SCS is particularly appealing due to its simplicity, low energy requirements, and ability to ensure uniform molecular-level mixing.

Among the various modifications of the SCS method, the use of ordinary cellulose-based paper has already been proposed as a fuel for nanoparticle synthesis, where it is impregnated with inorganic precursors and then calcined in air to remove the cellulose matrix by combustion [6,7]. However, commercial paper usually contains additives-such as fillers, binders, and sizing agents-that can decompose or react during heat treatment, potentially introducing impurities into the final product. On the other hand, flash paper, made from nitrocellulose, is a fast-burning material commonly used in magic tricks and special effects. Although it has not been used before in nanoparticle synthesis *via* SCS, it shows promise as an alternative organic fuel for the process. Nitrocellulose combusts cleanly, producing only gaseous byproducts such as CO_2, H_2O, and N_2, leaving no solid residue. Additionally, the porous structure of paper may promote uniform distribution of precursors and aid in nanoparticle formation. This makes nitrocellulose a more appealing choice for combustion synthesis due to its cleaner burn and simpler composition.

One of the key advantages of using flash paper combustion for SCS nanoparticle synthesis is the remarkable speed and simplicity of the process. The method requires minimal equipment-just an aqueous bath of metal nitrate salts and nitrocellulose paper-making it both accessible and cost-effective for laboratory-scale applications. The combustion is extremely rapid, occurring within seconds, which allows for fast material production. Importantly, the process generates high localized temperatures that can promote the formation of well-crystallized nanoparticles. Like SCS, this method benefits from a self-sustained exothermic reaction,

meaning that once initiated, no external heating is necessary. This self-heating characteristic not only simplifies the setup but also improves energy efficiency by generating heat through an exothermic process. The minimal equipment requirements, energy production, and portability of the method make it particularly attractive for on-site exploratory research.

Nanoparticles represent a compelling alternative to traditional bulk pigments, offering superior color performance in various materials [8,9]. Their ultra-small size (< 100 nm) enables better dispersion and higher color strength. When embedded in protective matrices, these nanoparticles also demonstrate enhanced resistance to environmental stressors such as UV radiation and chemical degradation. As a result, they are particularly well-suited for high-performance, durable applications across a range of industries, including paints, coatings, inks, cosmetics, ceramics, glasses, and plastics.

Cobalt blue ($CoAl_2O_4$) has long been valued as a pigment for its vibrant color and remarkable chemical and thermal stability [10–12]. In a rough estimate, around 60,000 tonnes of pigment are produced globally each year, representing approximately 3% of total cobalt mining, and are widely used in applications ranging from paints, ceramics, and glass to plastics, inks, optical devices, and catalysis. $CoAl_2O_4$ has a spinel crystal structure, with Co^{2+} ions located in tetrahedral sites-an arrangement that gives rise to its distinctive color. Because the color results from localized electronic transitions within the cobalt ions, it remains unaffected by particle size, eliminating visible quantum size effects. The pigment also demonstrates excellent thermal resistance, strong fade resistance, and environmental safety, making it a prominent candidate for developing durable and low-toxicity colorant systems. Nanoscale $CoAl_2O_4$ can be synthesized using several techniques, such as solid-state reactions, co-precipitation, microwave-assisted methods, solution combustion synthesis, and sol-gel processes [13–15]. These methods aim to produce cobalt blue pigments with reduced particle sizes, which enhance color strength and dispersibility. However, these approaches are often time- and energy-consuming, requiring prolonged high-temperature heating in box furnaces or microwave ovens, or the use of harsh reagents like strong bases during precipitation. Therefore, developing novel synthesis strategies that yield nanosized $CoAl_2O_4$ more rapidly and efficiently remains essential for advancing next-generation pigment technologies.

Along these lines, this study introduces, for the first time, a simple, rapid, and energy-efficient method for synthesizing cobalt blue pigment nanoparticles using flash paper combustion. The process involves immersing flash paper in an aqueous solution of the desired metal nitrates. After drying, the paper is ignited in air, where its rapid combustion generates a high local temperature that drives the decomposition of the precursor, yielding an inorganic residue containing nanoparticles of the target material. This technique is analogous to solution combustion synthesis (SCS), in which a fuel-oxidizer mixture undergoes an exothermic reaction to form nanoparticles. Like SCS, the flash paper method relies on a self-sustained thermal reaction that proceeds quickly after ignition without the need for external heating. Notably, the technique is inherently low-cost, uses readily available materials, and requires minimal infrastructure, offering a practical route for producing pigments without complex equipment. Its simplicity and efficiency suggest strong potential for larger-scale production, particularly in decentralized or resource-limited settings. Finally, the use of the as-synthesized nanoparticles in 3D printing formulations is also explored, enabling the creation of colored artifacts with diverse and complex designs.

2. Materials and Methods

2.1. Synthesis of cobalt blue nanoparticles

A salt bath solution was prepared by dissolving 26 g of aluminum nitrate nonahydrate [$Al(NO_3)_3 \cdot 9H_2O$, Aldrich] and 10 g of cobalt nitrate hexahydrate [$Co(NO_3)_2 \cdot 6H_2O$, Aldrich] in 100 mL of deionized water, maintaining a 2:1 molar ratio appropriate for forming spinel $CoAl_2O_4$. Rectangular pieces of thin flash paper made of nitrocellulose (6 cm x 9.5 cm, MagicStar, Keratsini, Greece) were immersed in this solution for a few seconds, then removed and drained. The drained pieces were suspended using small wooden clips and dried in an oven at 90°C for 45 minutes. The dried samples were subsequently ignited using a lighter in a porcelain crucible, initiating rapid, self-sustained combustion. This process yielded within a few seconds a lightweight, blue, fluffy solid identified as cobalt blue pigment, with an approximate yield of 20-30 mg per flash paper piece. The solid was not attracted to a magnet, in line with the antiferromagnetic nature of cobalt blue and its very weak room-temperature magnetism (*ca.* 10^{-3}-10^{-2} emu g^{-1}), resulting from partial substitution of aluminum by cobalt in octahedral sites.

Safety Note: The flash paper used in this work is a material commonly employed in magic tricks and effects demonstrations; it ignites rapidly and cleanly without explosion, ensuring safe handling and use.

2.2. Characterization techniques

X-ray diffraction (XRD) patterns were obtained on a Bruker D8 Advance diffractometer (Bruker AXS GmbH, Karlsruhe, Germany), using Cu Kα radiation at 36 kV / 36 mA. The instrument configuration included a 0.6 mm divergence slit, 2.5° primary and secondary Soller slits, a Ni Kβ filter and a high performance SSD160-2 detector. Samples were loaded on a silicon low-background holder and scanned from 2 to 80° 2θ, in steps of 0.02° 2θ, at a rate of 0.5 s per step. The DIFFRAC.EVA software (Bruker AXS GmbH, Karlsruhe, Germany) and the ICDD (International Centre for Diffraction Data) PDF-2 (2022) database were used for phase identification.

Quantitative phase analysis was performed by Rietveld refinement of the XRD data employing BGMN with Profex v.5.5.0 as a graphical user interface [16,17]. Experimental parameters, such as the goniometer radius, the type of X-ray source, the primary and secondary beam optics, the sample geometry and the detector model, were specified in order to accurately reproduce the measured peak shape. The crystallite size, micro-strain and preferred orientation were refined in the selected structure files, while the background shape was optimized by varying its polynomial degree. The quality of refinements was assessed through the "goodness of fit (GOF)", a statistical measure generated by BGMN/Profex; a GOF value in the range 1.0-2.0 indicates a good agreement between measured and calculated patterns.

Transmission electron microscopy (TEM) observations were performed using the JEM HR-2100 microscope (JEOL Ltd., Tokyo, Japan) operated at 200 kV in bright-field mode. A drop of ethanol, containing the ultrasonically dispersed particles, was placed onto a holey carbon film supported by a copper-mesh TEM grid (CF300-CU-UL, carbon square mesh, CU, 300 mesh from Electron Microscopy Science, Hatfield, UK) and it was air-dried at room temperature. The elemental composition of the sample was obtained using a JEOL JSM 6510-LV, SEM Microscope instrument (JEOL Ltd., Tokyo, Japan) equipped with an X-Act EDS-detector from Oxford Instruments (Abingdon, Oxfordshire, UK) for energy dispersive X-ray spectroscopy with an acceleration voltage of 20 kV.

Nitrogen (N_2) adsorption-desorption isotherms were measured by an ASAP 2460 analyzer (Micromeritics, Norcross, GA, USA) by using ultrahigh pure N_2 (99.999%). The sample was outgassed for 10 h under vacuum (10^{-4} mbar) at 120°C. Porosimetry isotherms were recorded at 77 K using a liquid N_2 Dewar vessel at a relative pressure (P/P_o) of 10^{-2} to 0.99.

2.3. Color 3D printing formulations

A nanoputian molecule was selected as a model to showcase the use of cobalt blue nanopigment in colored photoactive resin formulations for 3D printing applications. The molecular coordinates of the nanoputian molecule, commonly referred to as nanokid, were retrieved in SDF format from National Center for Biotechnology Information (2025), PubChem Compound Summary for CID 11353257, Nanoputian (retrieved July 9, 2025 from https://pubchem.ncbi.nlm.nih.gov/compound/Nanoputian). A custom Python script was developed to remove hydrogen atoms from the SDF file which was then converted into a 3D mesh in STL format using the Jmol molecular modeling software (http://www.jmol.org/). Two types of 3D models were generated in Jmol: i) a stick representation and ii) a space-filling representation. The STL files were subsequently imported into the NovaMaker 3D printing software, which is compatible with the Nova 3D resin photopolymer printer used for printing the models (Shenzhen Nova Robot Technology Co., Ltd., Shenzhen, China). To colorize the clear resin, 4 mL of a pre-prepared dispersion containing 1 wt.% cobalt blue pigment-dispersed *via* sonication-was added to 100 mL of Copymaster3D Standard Clear resin (https://copymaster3d.com/). This resulted in a final concentration of 0.04 wt.% cobalt blue in the mixture. For visual comparison purposes, the nanokid model was 3D printed using both uncolored resin and resin tinted with cobalt blue pigment.

3. Results and Discussion

3.1. Synthesis and characterization of cobalt blue nanoparticles

To synthesize cobalt aluminate ($CoAl_2O_4$), a salt bath containing aluminum and cobalt nitrates was prepared in proportions suitable for forming the spinel phase. Substrates made of flash paper were immersed in this solution, followed by drying under mild heating conditions. Upon ignition with a lighter, a rapid, self-sustained combustion reaction occurred, approximated by the following balanced reaction [1] (assuming the average nitrocellulose composition as $C_6H_{7.6}O_{8.4}N_{2.4}$ [18]):

$$Co(NO_3)_2{\cdot}6H_2O + 2Al(NO_3)_3{\cdot}9H_2O + 3C_6H_{7.6}O_{8.4}N_{2.4} \rightarrow CoAl_2O_4 + 7.6N_2 + 18CO_2 + 35.4H_2O$$

The process produced a lightweight solid within seconds as nitrates and nitrocellulose were converted into gaseous products (N_2, CO_2, H_2O), displaying the distinct cobalt blue pigment coloration (Fig. 1, top). Using the molar enthalpies of formation for the reactants and products in the balanced reaction above, the reaction is determined to be exothermic, releasing approximately 5 MJ of energy per mole of $CoAl_2O_4$ formed-sufficient to boil and fully vaporize around 2 liters of water. This value is an order of magnitude greater than the energy released during industrial H_2SO_4 synthesis (*ca.* 0.5 MJ per mol), a key chemical in industry, where the heat is partially recovered as useful work-primarily through steam generation that drives turbines to produce electricity. Alternatively, the thermochemical data correspond to roughly 7 kJ of energy released per gram of nitrocellulose-nearly double its typical energy density of 3.5-4 kJ g^{-1} [19]. Hence, the presence of nitrate salts appears to enhance the combustion performance of nitrocellulose, leading to a higher energy release. Evidently, thermal camera recordings showed that the temperature developed by burning nitrocellulose was lower than that of burning nitrate-impregnated nitrocellulose (360°C *vs.* 420°C) (Fig. 1, bottom), although local temperatures may exceed these values.

The XRD pattern reveals that the sample consists predominantly of cobalt aluminate ($CoAl_2O_4$) with a minor presence of cobalt(II) oxide (CoO) (Fig. 2). Phase identification was performed by comparing the experimental pattern with standard reference patterns from the PDF database: $CoAl_2O_4$ (PDF 00-010-0458) and CoO (PDF 00-048-1719). The major phase is identified as $CoAl_2O_4$, a spinel-structured material with a cubic crystal system (space group Fd-3m). Its characteristic diffraction peaks are observed at approximately 2θ = 31.3°, 36.9°, 44.8°, 55.6°, 59.4°, and 65.2°, corresponding to the (220), (311), (400), (422), (511), and (440) planes, respectively [20–22]. The sharpness and intensity of these peaks indicate a high degree of crystallinity in the spinel phase. In addition to the spinel phase, a lower-intensity peak is observed at around 2θ = 42.4°, corresponding to the main CoO (200) reflection. This suggests the presence of CoO, likely formed through thermal disproportionation of the spinel phase during high-temperature processing [23,24]. Quantitative phase analysis using the Rietveld refinement method confirms that the sample contains approximately 96 wt.% $CoAl_2O_4$ and 4 wt.% CoO (Table 1).

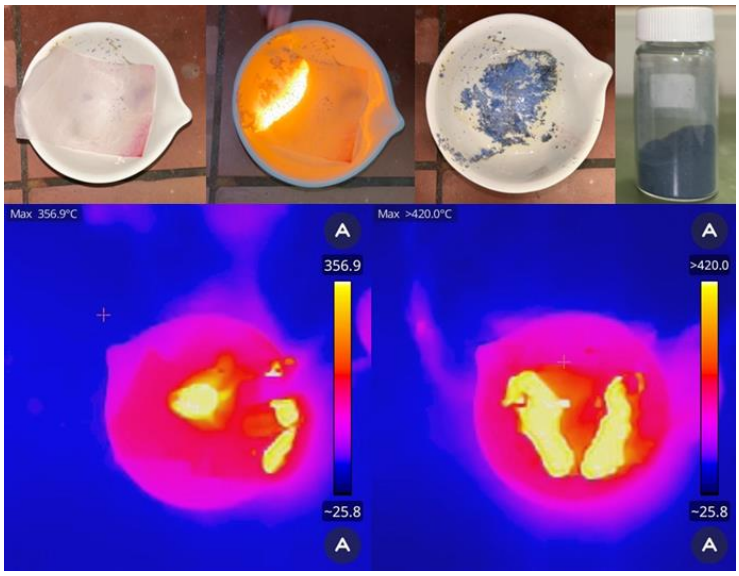

Fig. 1. (**Top**) Left to right: Flash paper infused with nitrate salts is ignited using a lighter in a porcelain crucible, triggering self-sustained combustion that produces a lightweight cobalt blue pigment within seconds. The far-right photo shows a vial containing the bulk quantity of cobalt blue nanopowder (1-1.5 g) obtained after multiple repetitions of the flash paper combustion synthesis process. (**Bottom**) Thermal camera images capturing the peak temperatures during the ignition of parent nitrocellulose (left) and nitrate-impregnated nitrocellulose (right). The parent nitrocellulose reached a maximum temperature of 360°C, while the nitrate-impregnated sample peaked at 420°C.

Table 1. Phase analysis obtained by Rietveld refinement of the XRD patterns.

			Composition	
Sample	**Phase**	**PDF-2 code**	**(wt.%)**	**GOF***
$CoAl_2O_4$	$CoAl_2O_4$	00-010-0458	96	1.18
	CoO	00-048-1719	4	
Cr_2O_3	Cr_2O_3	00-006-0504	100	1.53
γ-Fe_2O_3	γ-Fe_2O_3	01-076-3169	83	0.19
	FeO	01-080-3819	17	
$CoFe_2O_4$	$CoFe_2O_4$	00-022-1086	29	1.37
	CoO	00-048-1719	71	
$NiFe_2O_4$	$NiFe_2O_4$	01-071-3850	86	1.38
	Ni	00-004-0850	14	

* Goodness of fit, calculated by BGMN/Profex.

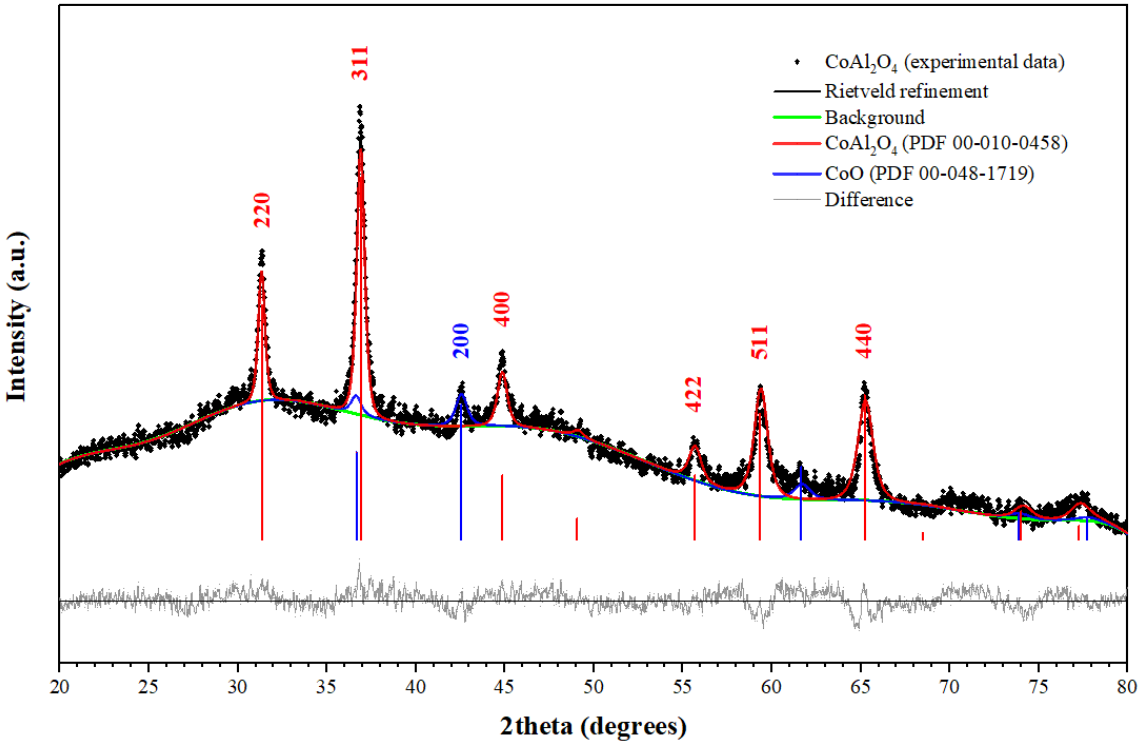

Fig. 2. The XRD pattern of the as-synthesized cobalt blue nanoparticles is presented along with its Rietveld refinement. The experimental data are represented by black dots, the fitted curve by a solid line, and the difference plot is displayed in grey at the bottom. The contributions of $CoAl_2O_4$ (red) and CoO (blue) phases are indicated, with corresponding Bragg reflection positions marked according to PDF cards.

The lattice constant of the $CoAl_2O_4$ spinel phase was determined from the XRD pattern using Bragg's law in combination with the geometry of the cubic spinel structure. Several prominent diffraction peaks were selected and indexed based on the characteristic reflections of $CoAl_2O_4$, specifically the (220), (311), (400), (511), and (440) planes. For each peak, the interplanar spacing (d_{hkl}) was calculated using the Bragg equation, $d_{hkl} = \lambda / 2 \sin\theta$, with $\lambda = 1.54$ Å (Cu Kα radiation). The corresponding lattice constant α was then computed using the cubic relationship [25]:

$$\alpha = d_{hkl} \cdot (h^2 + k^2 + l^2)^{1/2}$$

The values obtained from the individual peaks were averaged to enhance accuracy. The resulting average lattice constant was found to be 8.080 Å, which is in excellent agreement with the standard literature value of 8.086 Å for $CoAl_2O_4$. This confirms the presence of a well-crystallized spinel phase with structural parameters consistent with those reported for pure cobalt aluminate. The small lattice shrinkage from 8.086 Å to 8.080 Å (*ca.* 0.1%) is most likely due to partial cation inversion, oxygen non-stoichiometry, and the formation of a secondary CoO phase, which may lead to a depletion of Co^{2+} ions from the spinel lattice.

The Scherrer equation is a fundamental formula used in XRD analysis to estimate the size of crystalline domains (also known as crystallite size) in a material. It is expressed as [25,26]:

$$D = K \lambda / \beta \cos\theta$$

where D is the average crystallite size, K is the shape factor (around 0.9 for spherical crystals of cubic symmetry), λ is the wavelength of the X-ray source, β is the full width at half maximum (FWHM) of the diffraction peak (in radians), and θ is the Bragg angle. The equation assumes that the broadening of diffraction peaks is primarily due to the small size of the crystallites. Though it provides only an approximate value, the Scherrer equation is widely used due to its simplicity and effectiveness in analyzing nanocrystalline materials. In the present case, the equation was applied for $CoAl_2O_4$ to the most intense diffraction peak, identified as the (311) plane, to estimate the crystallite size of the spinel. Using the values $\theta = 18.4°$, $\beta = 8.95 \cdot 10^{-3}$ radians, and an X-ray wavelength $\lambda = 0.154$ nm, and assuming a shape factor $K = 0.9$, the calculated crystallite size D is approximately 16 nm. This result indicates that cobalt blue pigment possesses nanoscale crystalline domains.

TEM reveals that the nanoparticles exhibit a nearly spherical morphology, with individual particle sizes ranging from approximately 19 to 25 nm and an average size around 20 nm (Fig. 3, top). This is in good agreement with the crystallite size of 16 nm previously estimated from the Scherrer equation applied to XRD data, suggesting consistent structural characterization across techniques. Energy-dispersive X-ray spectroscopy (EDS) analysis (Fig. 3, bottom) confirms the elemental composition of the sample, showing a uniform spatial distribution of cobalt (Co), aluminum (Al), and oxygen (O) throughout the material. According to EDS analysis, the weight percentages of the elements in the sample are Co (45%), Al (40%), and O (15%), whereas the theoretical values for $CoAl_2O_4$ are Co (33%), Al (31%), and O (36%). The lower EDS analysis percentage of oxygen compared to the theoretical value [27] may be attributed to absorption and matrix effects inherent to low energy X-rays, such as the 0.52 keV oxygen Kα1 emission. Such effects are expected to reduce the oxygen peak intensity and, despite elaborate software corrections, may lead to an underestimation of oxygen and a concomitant overestimation of heavier elements (*i.e.*, aluminum and cobalt) concentrations present in the sample. However, the Co:Al mass ratio based on both EDS analysis and theoretical calculations is close to 1.1, corresponding to an atomic ratio of Co:Al = 0.5 in both cases. Overall, elemental mapping supports the successful synthesis of cobalt aluminate with homogenous phase composition.

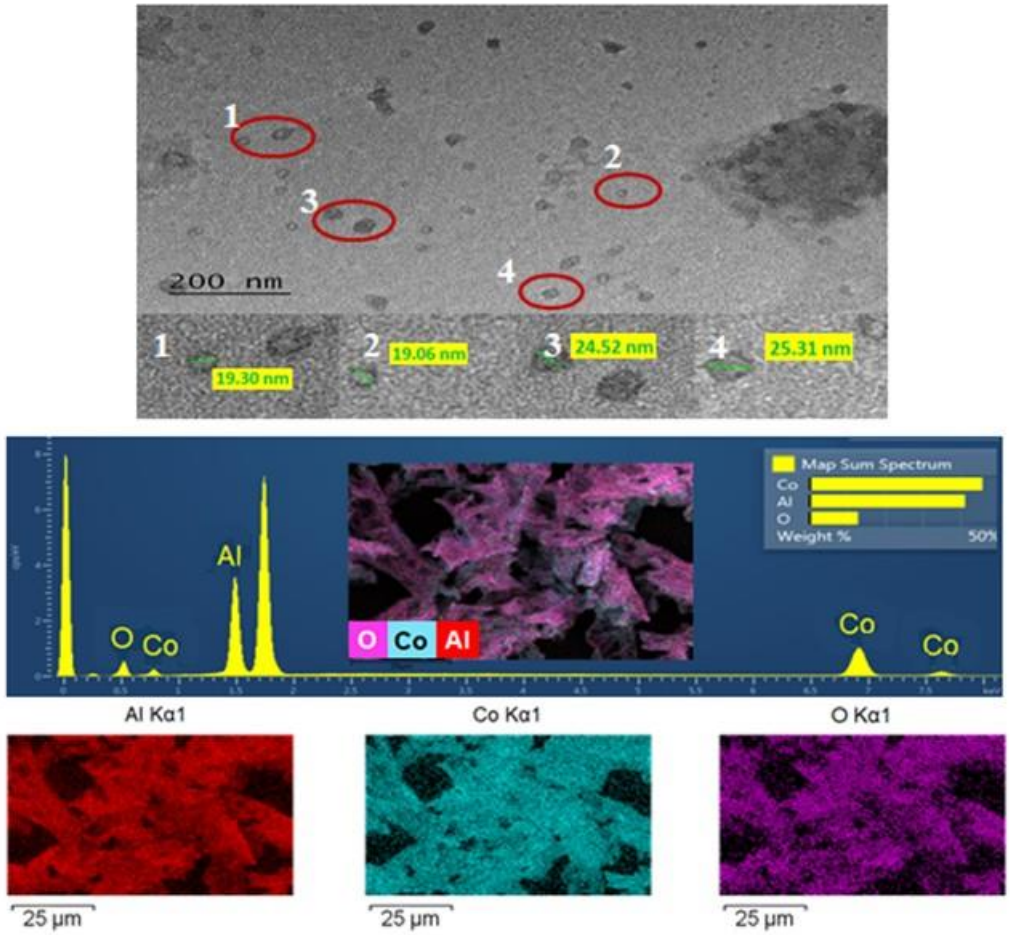

Fig. 3. (**Top**) TEM image of cobalt aluminate nanoparticles with four magnified sections showing particle sizes ranging from 19 to 25 nm. (**Bottom**) EDS elemental spectrum acquired on a Si substrate and associated element maps.

To gain deeper insight into the pore structure of the material, nitrogen porosimetry measurements were conducted. The shape of the resulting hysteresis loop (Fig. 4, left) clearly corresponds to an H3-type [28,29], indicating that the material comprises non-rigid aggregates of particles and includes a portion of macropores that are not fully saturated with pore condensate. The porosimetry data were analyzed using the corrugated pore structure model (CPSM) and the Brunauer-Emmett-Teller (BET) model [30]. The BET-specific surface area was determined to be 51 $m^2 g^{-1}$, closely aligning with the 53 $m^2 g^{-1}$ value predicted by the CPSM simulation. This consistency is attributed to the absence of micropores and the predominance of pores larger than 10 nm, in agreement with a previous study [30]. Furthermore, the CPSM simulation estimated the total pore volume at 0.177 $cm^3 g^{-1}$. Based on the pore volume distribution shown in Fig. 4, right, the mean pore diameter was calculated as 14 nm.

Interestingly, the specific surface area (SSA) of spherical nanoparticles can be estimated using the formula SSA = 6 / ρ·d, where ρ is the true material density (g cm^{-3}) and d is the particle diameter (cm). This relationship is derived from the surface-to-volume ratio of spheres and is widely used in materials science [31,32]. For cobalt blue nanoparticles with a TEM-determined size of approximately 20 nm ($2.0 \cdot 10^{-6}$ cm) and a true density of approximately 4.2 g cm^{-3}, the theoretical SSA is calculated as 71 m^2 g^{-1}. This value represents the highest specific surface area possible under ideal, non-aggregated conditions and acts as a benchmark for comparing the experimental BET measurement of 51 m^2 g^{-1}, suggesting that the nanoparticles show a moderate level of aggregation due to the fluffy nature of the lightweight solid.

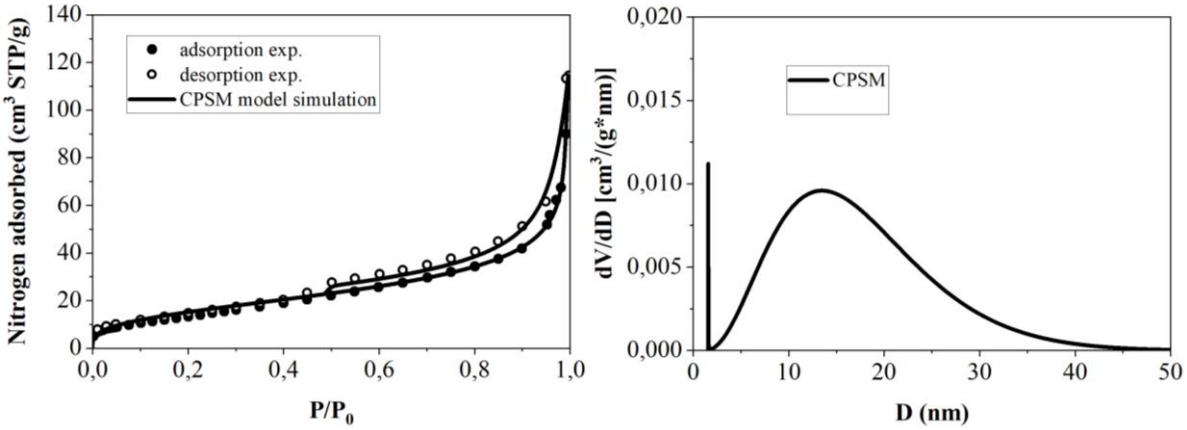

Fig. 4. (**Left**) Experimental data from nitrogen porosimetry (discrete points) alongside CPSM model simulation (solid line). (**Right**) Differential pore volume distribution as predicted by the CPSM model.

In summary, cobalt blue nanoparticles were rapidly synthesized *via* self-sustained ignition of nitrocellulose-based flash paper impregnated with the corresponding nitrate salts. The resulting nanoparticles are crystalline, exhibit nearly spherical morphology (20 nm by TEM), and possess a relatively high surface area of 51 m^2 g^{-1}.

3.2. Generality and scale-up potential

The method can be generalized to other types of pigments, as evidenced through a series of trials using suitable inorganic precursors (purchased from Aldrich). For instance, chromium(VI) oxide (20 g of CrO_3 in 100 mL H_2O) was used to obtain green Cr_2O_3 (Figs 5 & 6). On the other hand, iron(III) nitrate nonahydrate alone (28 g iron salt in 100 mL H_2O) or in combination with either cobalt(II) nitrate hexahydrate (28 g iron salt & 10 g cobalt salt in 100 mL H_2O) or nickel(II) nitrate hexahydrate (28 g iron salt & 10 g nickel salt in 100 mL H_2O) yielded black magnetic pigments, *i.e.*, γ-Fe_2O_3, $CoFe_2O_4$, or $NiFe_2O_4$, respectively (Fig. 6). For γ-Fe_2O_3, the presence of FeO is detected, likely resulting from the disproportionation of the initially formed magnetite (Fe_3O_4) spinel [23,24]. Similarly, for $CoFe_2O_4$, an additional phase corresponding to CoO is observed, attributed to the disproportionation of the spinel structure [23,24]. In the case of $NiFe_2O_4$, a metallic Ni phase is identified, which is ascribed to the side reduction of nickel ions by the cellulosic matrix during synthesis [33]. Table 1 summarizes the phase composition percentages in each sample as determined by Rietveld refinement. It should be noted that, in certain cases, such as the synthesis of $MgAl_2O_4$ and ZnO white pigments, incomplete combustion of the nitrocellulose matrix was observed. When starting from nitrate precursors impregnated into flash paper, the presence of magnesium or zinc ions appears to inhibit the full oxidation of nitrocellulose during the combustion process [34–36]. This interference results in residual carbon being deposited alongside the intended white pigments, diminishing the purity and brightness of the final product. All in all, these complementary results highlight the versatility of the method for synthesizing a range of inorganic pigments, while also stressing the importance of controlling reaction conditions to minimize the formation of secondary phases.

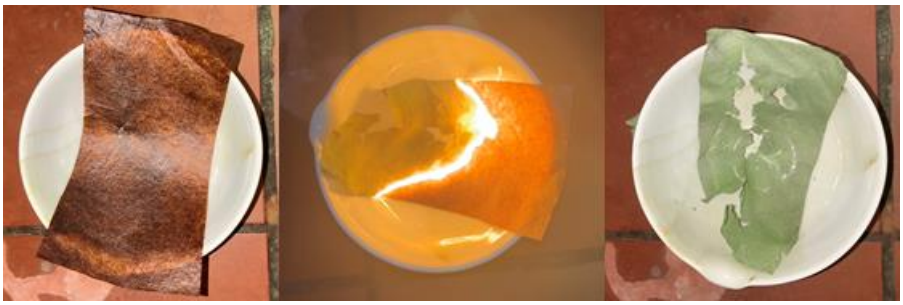

Fig. 5. Left to right: Flash paper infused with CrO_3 is ignited using a lighter in a porcelain crucible, triggering self-sustained combustion that produces a lightweight Cr_2O_3 green pigment within seconds.

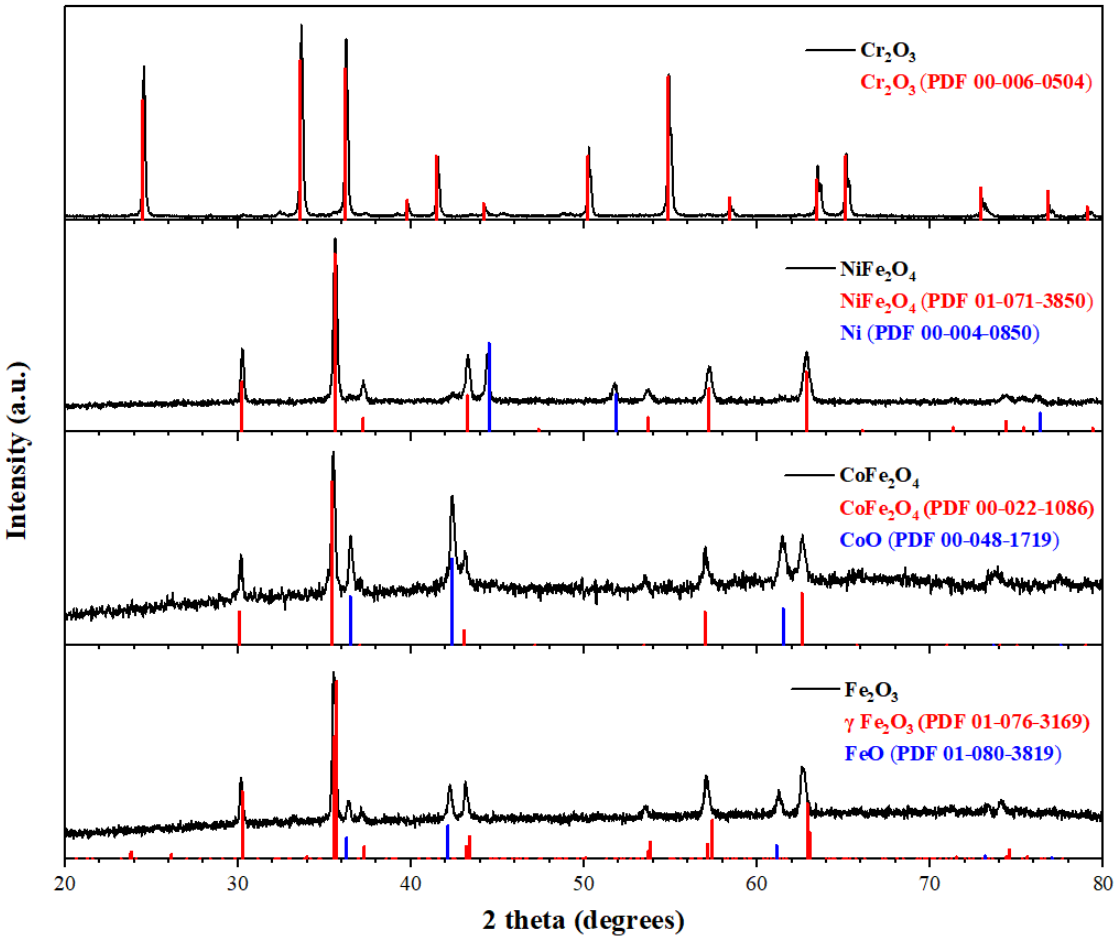

Fig. 6. XRD patterns of various synthesized metal oxide samples compared with standard reference patterns. Experimental patterns are shown in black, with reference peaks for primary phases in red and secondary phases in blue.

Although flash paper combustion is convenient at a small laboratory scale, scaling it for industrial applications requires an integrated, continuous system encompassing material treatment, controlled combustion, and energy recovery. In such a setup, rolls of nitrocellulose sheets could be continuously fed into a nitrate salt impregnation bath, containing metal nitrates. After impregnation, the sheets would be carefully dried using a multi-zone industrial oven. The dried, nitrate-infused flash paper could then be segmented and introduced into a pulse-controlled combustion chamber, where precisely timed ignitions would ensure efficient and complete combustion in short, controlled bursts. The heat released by this rapid exothermic reaction could be harnessed *via* a water-jacketed heat exchanger to generate steam, which would drive a turbine and convert thermal energy into electricity. Simultaneously, the solid residues-primarily metallic oxides-could be collected downstream for pigment extraction, thereby closing the loop on resource

recovery. This approach offers a scalable, continuous process that integrates materials processing, thermal energy harnessing, and pigment recovery.

3.3. Integration into color 3D printing

Cobalt blue-a pigment historically used in ceramics and fine arts-is employed here in the development of UV-curable 3D printing formulations for colored applications, highlighting the versatility of the as-made $CoAl_2O_4$ as a functional pigment across different materials and technologies. Its intense blue hue, chemical stability, and resistance to heat and light make it particularly valuable in artistic and industrial contexts. Moreover, its nanoscale size, high surface area, and low weight enable easy dispersion into photoactive resins *via* sonication, eliminating the need for any further post-treatment of the nanoparticles.

3D printing using UV curable resins, also known as stereolithography (SLA), is a high-precision additive manufacturing process [37]. It involves layer-by-layer curing of liquid photopolymer resin using UV light. When exposed to UV light, the resin undergoes a chemical reaction, solidifying into a hardened plastic. This technology enables the creation of highly detailed and complex parts with smooth surface finishes, making it suitable for a wide range of applications, including functional prototypes, custom components, artistic models, and various industrial and consumer products.

Colored 3D printing with UV-curable resins is achievable, enabling the creation of vibrant, fully colored models without additional post-processing [38]. This process involves mixing pigments into the resin, which must be compatible with the photopolymer and allow adequate UV light penetration for proper curing. However, the addition of pigments can influence the resin's curing depth and speed, so formulations must be carefully optimized to preserve both print quality and mechanical performance.

$CoAl_2O_4$ is not formally recognized as a UV blocker, but it can provide some incidental UV resistance when used as a pigment in UV-curable resins for 3D printing. Its inorganic, crystalline structure and relatively high refractive index (1.8 versus 1.5 for typical resin) contribute to partial UV opacity, primarily through the scattering of curing light. Similarly to other metal oxide pigments, $CoAl_2O_4$ is capable of both scattering and, to a limited extent, absorbing UV radiation [22,29,39]. This behavior is particularly important in UV-curable systems, where UV light is critical for initiating polymerization. A major challenge when formulating these resins with inorganic pigments like $CoAl_2O_4$ is maintaining adequate light transmission to ensure proper curing. To overcome this, the pigment concentration is kept as low as possible-often below 0.1 wt.%-to achieve sufficient color while minimizing interference with the curing process. The strong absorption coefficient of cobalt blue in the visible region supports this approach, allowing effective coloration even at low pigment loadings.

To demonstrate the feasibility of incorporating cobalt blue nanopigment into photoactive resin formulations for aesthetic 3D printing, a nanoputian molecule-commonly known as nanokid-was selected as a representative model due to its structurally complex, anthropomorphic geometry and public availability of molecular data [40]. Fig. 7 presents 3D printed models of the nanokid molecule rendered in both stick and ball-and-stick formats, produced using UV-curable resins formulated with and without cobalt blue nanoparticles. These prints not only demonstrate the feasibility of fabricating visually striking, geometrically complex molecular structures using pigmented photoresins, but also yield mechanically stable artifacts suitable for handling and display. To the best of our knowledge, this might constitute the first reported application of cobalt blue as a colorant in STL-based 3D printing, specifically for enhancing the aesthetic appeal of printed objects.

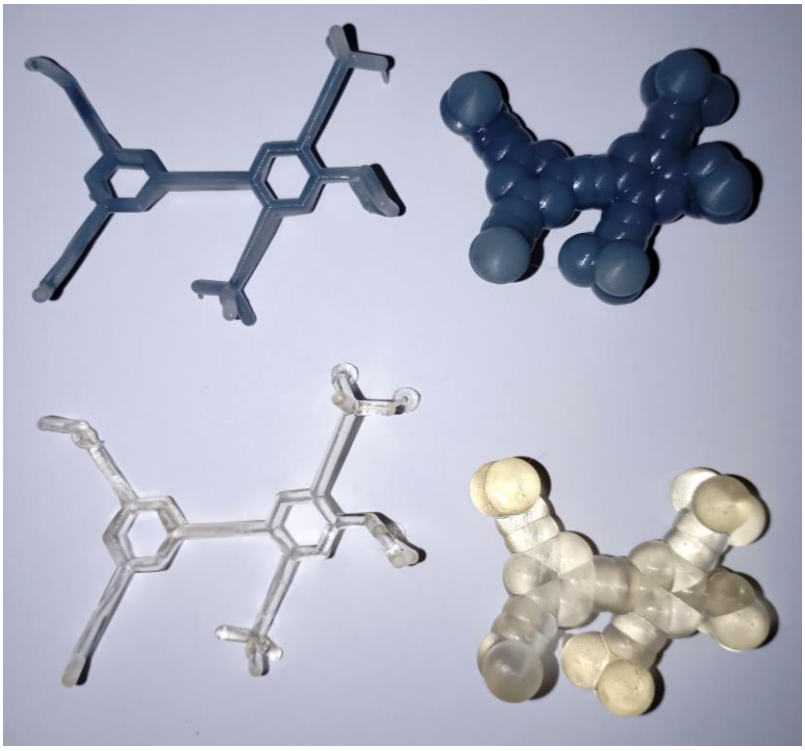

Fig. 7. 3D printed nanokid molecule models fabricated with UV-cured resins. Two molecular representations are shown: stick models (top left and bottom left) and ball-and-stick models (top right and bottom right). The stick models are printed using clear (bottom left) and colored (top left) UV-curable resin, with the colored version incorporating cobalt blue nanoparticles. Likewise, the ball-and-stick models use cobalt blue nanoparticle-infused resin (top right) and transparent resin (bottom right), highlighting differences in visualization. The printed articles measure 7 cm by 6 cm.

4. Conclusions

This study explores a novel synthesis route for cobalt blue ($CoAl_2O_4$) nanoparticles *via* nitrocellulose-based flash paper combustion, utilizing cobalt and aluminum nitrates as precursors. The process, resembling the solution combustion synthesis (SCS) method, involves the immersion of flash paper in an aqueous bath containing stoichiometrically balanced metal nitrates, followed by ignition under ambient conditions. Upon ignition, a rapid, self-sustained heating reaction occurs, facilitating the high-temperature formation of crystalline cobalt aluminate nanoparticles within a few seconds. The resulting $CoAl_2O_4$ nanocrystals exhibit nearly spherical morphology with an average diameter of 20 nm and high surface area (51 m^2 g^{-1}), characteristics that enhance their dispersion and performance in practical applications. This energy-efficient and time-saving synthesis method yields pigment-grade cobalt blue nanopowders ideal for incorporation into UV-curable 3D printing resins, offering vibrant coloration and stability. Importantly, the method is generalizable and can be extended to the synthesis of a broad range of mixed metal oxide nanoparticles by varying the composition in the precursor solution, offering a versatile platform for nanopigment production. Overall, flash paper combustion offers a rapid, user-friendly alternative to conventional high-temperature synthesis methods. Its simplicity and efficiency make it particularly well-suited for preliminary investigations and small-scale, on-site nanoparticle production, underscoring its potential as a valuable tool in materials research.

Author Contributions: conceptualization, A. B. Bourlinos; methodology, A. B. Bourlinos, A. Polymeros and C. Papachristodoulou; software, A. Polymeros and C. Papachristodoulou; validation, A. B. Bourlinos, A. Polymeros and C. Papachristodoulou; formal analysis, C. Papachristodoulou, D. Moschovas, A. Avgeropoulos and C. E. Salmas; investigation, A. B. Bourlinos, A. Polymeros and M. A. Karakassides; resources, A. B. Bourlinos, A. Polymeros, C. Papachristodoulou, A. Avgeropoulos, C. E. Salmas and M. A. Karakassides; data curation, A. B. Bourlinos, A. Polymeros and C. Papachristodoulou; writing-original draft preparation, A. B. Bourlinos, A. Polymeros, C. Papachristodoulou and C. E. Salmas; writing-review and editing, A. B. Bourlinos, A. Polymeros, C. Papachristodoulou, D. Moschovas, A. Avgeropoulos, C. E. Salmas and M. A. Karakassides; visualization, A. B. Bourlinos, A. Polymeros, C. Papachristodoulou, D. Moschovas and C. E. Salmas; supervision, A. B. Bourlinos. All authors have read and agreed to the published version of the manuscript.

Funding: This research did not receive external funding.

Data Availability Statement: The data of this study are available from the corresponding author upon reasonable request.

Conflicts of Interest: The authors declare no conflict of interest.

References

1. Varma, A.; Mukasyan, A.S.; Rogachev, A.S.; Manukyan, K.V. Solution combustion synthesis of nanoscale materials. *Chem. Rev.* **2016**, *116*, 14493–14586. https://doi.org/10.1021/acs.chemrev.6b00279
2. Xiao, X.; Li, Y.; Chen, N.; Xing, X.; Deng, D.; Wang, Y. Combustion agent mediated flash synthesis of porous MCo_2O_4 (M = Zn, Ni, Cu and Fe) via self-sustained decomposition of metal-organic complexes. *Mater. Lett.* **2017**, *195*, 123–126. https://doi.org/10.1016/j.matlet.2017.02.110
3. Han, M.; Wang, Z.; Xu, Y.; Wu, R.; Jiao, S.; Chen, Y.; Feng, S. Physical properties of $MgAl_2O_4$, $CoAl_2O_4$, $NiAl_2O_4$, $CuAl_2O_4$, and $ZnAl_2O_4$ spinels synthesized by a solution combustion method. *Mater. Chem. Phys.* **2018**, *215*, 251–258. https://doi.org/10.1016/j.matchemphys.2018.05.029
4. Gyulasaryan, H.; Kuzanyan, A.; Manukyan, A.; Mukasyan, A.S. Combustion synthesis of magnetic nanomaterials for biomedical applications. *Nanomaterials* **2023**, *13*, 1902. https://doi.org/10.3390/nano13131902
5. Padayatchee, S.; Ibrahim, H.; Friedrich, H. B.; Olivier, E. J.; Ntola, P. Solution combustion synthesis for various applications: A review of the mixed-fuel approach. *Fluids* **2025**, *10*, 82. https://doi.org/10.3390/fluids10040082
6. Lennon, E.M.; Tanzy, M.C.; Volpert, V.A.; Mukasyan, A.S.; Bayliss, A. Combustion of reactive solutions impregnated into a cellulose carrier: modeling of two combustion fronts. *Chem. Eng. J.* **2011**, *174*, 333–340. https://doi.org/10.1016/j.cej.2011.04.005
7. Danghyan, V.; Orlova, T.; Roslyakov, S.; Wolf, E. E.; Mukasyan, A. S. Cellulose assisted combustion synthesis of high surface area Ni–MgO catalysts: mechanistic studies. *Combust. Flame* **2020**, *221*, 462–475. https://doi.org/10.1016/j.combustflame.2020.08.026
8. Cavalcante, P.M.T.; Dondi, M.; Guarini, G.; Raimondo, M.; Baldi, G. Colour performance of ceramic nano-pigments. *Dyes Pigm.* **2009**, *80*, 226–232. https://doi.org/10.1016/j.dyepig.2008.07.004
9. Shah, K.W.; Huseien, G.F.; Kua, H.W. A state-of-the-art review on core–shell pigment nanostructure preparation and test methods. *Micro* **2021**, *1*, 55–85. https://doi.org/10.3390/micro1010006
10. Smith, C.A. Blue pigment review. *Pigment Resin Technol.* **1984**, *13*, 14–24. https://doi.org/10.1108/eb042058
11. Duell, B. A.; Li, J.; Subramanian, M. A. Hibonite blue: A new class of intense inorganic blue colorants. *ACS Omega* **2019**, *4*, 22114-22118. https://doi.org/10.1021/acsomega.9b03255
12. Ruiz-Moreno, S.; Soneira, M.; Perez-Pueyo, R. Practical identification of cobalt-based blue pigments detecting the induced photoluminescence by a He–Ne laser using a Raman spectrometer. *J. Raman Spectrosc.* **2024**, *55*, 299–304. https://doi.org/10.1002/jrs.6636
13. Zayat, M.; Levy, D. Blue $CoAl_2O_4$ particles prepared by the sol–gel and citrate-gel methods. *Chem. Mater.* **2000**, *12*, 2763–2769. https://doi.org/10.1021/cm001061z
14. Paulo-Redondo, G.; Nebot-Díaz, I. Study of the synthesis variables in the preparation of $CoAl_2O_4$ pigment using microwaves to reduce energetic consumption. *Eng* **2023**, *4*, 2826–2839. https://doi.org/10.3390/eng4040159
15. Chavarriaga, E.A.; Wermuth, T.B.; Arcaro, S.; García, C.; Ramirez, M.A.; Gómez, A.; Bezzon, V.D.N.; Orlando, M.T.D.; Alarcón, J.; Bergmann, C.P.; Lopera, A.A. One-step synthesis of $CoAl_2O_4$ inorganic pigment by solution combustion: The impact of fuel and ammonium nitrate. *Ceram. Int.* **2024**, *50*, 45–54. https://doi.org/10.1016/j.ceramint.2023.09.205
16. Bergmann, J.; Friedel, P.; Kleeberg, R. BGMN: A new fundamental parameters based Rietveld program for laboratory X-ray sources, its use in quantitative analysis and structure investigations. *CPD Newslett.* **1998**, *20*, 5–8.
17. Döbelin, N.; Kleeberg, R. Profex: A graphical user interface for the Rietveld refinement program BGMN. *J. Appl. Crystallogr.* **2015**, *48*, 1573–1580. https://doi.org/10.1107/S1600576715014685
18. Morris, E.; Pulham, C.R.; Morrison, C.A. Structure and properties of nitrocellulose: Approaching 200 years of research. *RSC Adv.* **2023**, *13*, 32321–32333. https://doi.org/10.1039/D3RA05457H
19. Yolhamid, M.N.A.G.; Ibrahim, F.; Amir, M.A.U.; Ibrahim, R.; Adnan, S.; Yahya, M.Z.A. The processing of nitrocellulose from rhizophora, palm oil bunches (EFB) and kenaf fibres as a propellant grade. *Int. J. Eng. Technol.* **2018**, *7*, 59–65. https://doi.org/10.14419/ijet.v7i4.29.21844
20. Duan, X.; Pan, M.; Yu, F.; Yuan, D. Synthesis, structure and optical properties of $CoAl_2O_4$ spinel nanocrystals. *J. Alloys Compd.* **2011**, *509*, 1079–1083. https://doi.org/10.1016/j.jallcom.2010.09.199
21. Irfan, H.; Racik, K.M.; Anand, S. X-ray peak profile analysis of $CoAl_2O_4$ nanoparticles by Williamson–Hall and size–strain plot methods. *Mod. Electron. Mater.* **2018**, *4*, 31–40. https://doi.org/10.3897/j.moem.4.1.33272

22. Gingasu, D.; Mindru, I.; Culita, D.C.; Marinescu, G.; Somacescu, S.; Ianculescu, A.; Surdu, V.-A.; Preda, S.; Oprea, O.; Vasile, B.S. *Mentha piperita*-mediated synthesis of cobalt aluminate nanoparticles and their photocatalytic activity. *J. Mater. Sci.: Mater. Electron.* **2021**, *32*, 11220–11231. https://doi.org/10.1007/s10854-021-05791-z
23. Liebermann, R.C.; Jackson, I.; Ringwood, A.E. Elasticity and phase equilibria of spinel disproportionation reactions. *Geophys. J. Int.* **1977**, *50*, 553–586. https://doi.org/10.1111/j.1365-246X.1977.tb01335.x
24. Desautels, R.D.; van Lierop, J.; Cadogan, J.M. Disproportionation of cobalt ferrite nanoparticles upon annealing. *J. Phys. Conf. Ser.* **2010**, *217*, 012105. https://doi.org/10.1088/1742-6596/217/1/012105
25. Padmapriya, G.; Ananthi, K. Green synthesis and characterization studies of spinel $CoAl_2O_4$ nano-catalysts by microwave combustion method. *Malaya J. Mat.* **2020**, *2*, 2183–2186. https://doi.org/10.26637/MJM0S20/0561
26. Zhang, W.; Li, Z.; Wu, G.; Wu, W.; Zeng, H.; Jiang, H.; Zhang, W.; Wu, R.; Xue, Q. Effects of coloration of spinel $CoAl_2O_4$ cobalt blue pigments: Composition, structure, and cation distribution. *Inorganics* **2023**, *11*, 368. https://doi.org/10.3390/inorganics11090368
27. Ibrahim, M.A.; El-Araby, R.; Abdelkader, E.; El Saied, M.; Abdelsalam, A.M.; Ismail, E.H. Waste cooking oil processing over cobalt aluminate nanoparticles for liquid biofuel hydrocarbons production. *Sci. Rep.* **2023**, *13*, 3876. https://doi.org/10.1038/s41598-023-30828-0
28. Thommes, M.; Kaneko, K.; Neimark, A.V.; Olivier, J.P.; Rodriguez-Reinoso, F.; Rouquerol, J.; Sing, K.S.W. Physisorption of gases, with special reference to the evaluation of surface area and pore size distribution (IUPAC Technical Report). *Pure Appl. Chem.* **2015**, *87*, 1051–1069. https://doi.org/10.1515/pac-2014-1117
29. Fardood, S. T.; Moradnia, F.; Ganjkhanlu, S.; Ouni, L.; Ramazani, A.; Sillanpää, M. Green synthesis and characterization of spinel $CoAl_2O_4$ nanoparticles: Efficient photocatalytic degradation of organic dyes. *Inorg. Chem. Commun.* **2024**, *167*, 112719. https://doi.org/10.1016/j.inoche.2024.112719
30. Salmas, C.E.; Androutsopoulos, G.P. Rigid sphere molecular model enables an assessment of the pore curvature effect upon realistic evaluations of surface areas of mesoporous and microporous materials. *Langmuir* **2005**, *21*, 11146–11160. https://doi.org/10.1021/la0508644
31. Gallet, J.-C.; Domine, F.; Zender, C.S.; Picard, G. Measurement of the specific surface area of snow using infrared reflectance in an integrating sphere at 1310 and 1550 nm. *Cryosphere* **2009**, *3*, 167–182. https://doi.org/10.5194/tc-3-167-2009
32. Granados, N.B.; Yi, E.; Laine, R.; Baena, O.J.R. $CoAl_2O_4$ blue nanopigments prepared by liquid-feed flame spray pyrolysis method. *Rev. Mater.* **2015**, *20*, 580–587. https://doi.org/10.1590/S1517-707620150003.0059
33. Ma, B.; Chaudhary, J.P.; Zhu, J.; Sun, B.; Huang, Y.; Sun, D. Ni nanoparticle–carbonized bacterial cellulose composites for the catalytic reduction of highly toxic aqueous Cr(VI). *J. Mater. Sci.: Mater. Electron.* **2020**, *31*, 7044–7052. https://doi.org/10.1007/s10854-020-03270-5
34. Durin-France, A.; Ferry, L.; Lopez-Cuesta, J.-M.; Crespy, A. Magnesium hydroxide/zinc borate/talc compositions as flame-retardants in EVA copolymer. *Polym. Int.* **2000**, *49*, 1101–1105. https://doi.org/10.1002/1097-0126(200010)49:10<1101::AID-PI523>3.0.CO;2-5
35. Uzoma, P.C.; Obidiegwu, M.U.; Ezeh, V.O.; Akanbi, M.N.; Onuoha, F.N. The effect of magnesium hydroxide/zinc borate and magnesium hydroxide/melamine flame retardant synergies on polypropylene. *Int. J. Eng. Sci.* **2014**, *3*, 63–68.
36. Fayyadh, S.M.; Ahmed, A.B. A comparative study between the use of nanoparticles of magnesium oxide and zinc oxide as coating for polymeric surfaces: A flame retardant and corrosion resistance. *Mater. Chem. Phys.* **2024**, *314*, 128899. https://doi.org/10.1016/j.matchemphys.2024.128899
37. Jandyal, A.; Chaturvedi, I.; Wazir, I.; Raina, A.; Haq, M.I.U. 3D printing: A review of processes, materials and applications in Industry 4.0. *Sustain. Oper. Comput.* **2022**, *3*, 33–42. https://doi.org/10.1016/j.susoc.2021.09.004
38. Cheng, Y.-L.; Huang, K.-C. Preparation and characterization of color photocurable resins for full-color material jetting additive manufacturing. *Polymers* **2020**, *12*, 650. https://doi.org/10.3390/polym12030650
39. Mosleh, M. Auto-combustion preparation and characterization of $CoAl_2O_4$ nanoparticles with different morphologies and its photocatalyst application. *J. Mater. Sci.: Mater. Electron.* **2017**, *28*, 773–777. https://doi.org/10.1007/s10854-016-5589-8
40. Chanteau, S.H.; Tour, J.M. Synthesis of anthropomorphic molecules: The nanoputians. *J. Org. Chem.* **2003**, *68*, 8750–8766. https://doi.org/10.1021/jo0349227